Near-field Optical Spectroscopy and Microscopy of Laterally Coupled Quantum Dots: Bonding and Antibonding States

Young-Jun Yu, Haneol Noh, Gun Sang Jeon, and Wonho Jhe*

School of Physics and Astronomy, Seoul National University, Seoul 151-747, Korea

Yasuhiko Arakawa

Research Center for Advanced Science and Technology,

University of Tokyo, Tokyo 153-8505, Japan

(Dated: February 6, 2008)

Abstract

We report on high-resolution photoluminescence (PL) spectroscopic and microscopic study of *laterally coupled* InAs/GaAs self-assembled quantum dots by using a low-temperature near-field scanning optical microscope. We have observed slightly split PL spectra, which are associated with the bonding (symmetric) and antibonding (antisymmetric) energy states between two coupled quantum dots, closely located each other as confirmed by spatial mapping of the PL intensity. The experimental results are in qualitative agreement with the simple theoretical calculations based on a two-dimensional potential model. This work may open the way to a *simultaneous* spectroscopy and microscopy study of laterally coupled quantum dots in a *high-density* quantum dot sample without any articulate sample fabrication.

PACS numbers: 68.37.Uv, 78.55.Cr, 78.67.Hc, 73.21.La

*Corresponding author: whjhe@snu.ac.kr

Any coupled single quantum systems, from atoms to molecules to quantum dots to macro-objects, feature split energy states. For example, the positively charged hydrogen molecule H_2^+ exhibits energy splitting into the bonding and antibonding states associated with, respectively, the symmetric and antisymmetric wave-functions between two neighboring nuclei [1]. For semiconductor quantum dots (QDs), the observation of the split energies due to coupled QDs or 'artificial molecules' has been also made and the mechanism of an exciton bound to the split energy states of coupled QDs can be understood by an analogy with the ionized hydrogen molecules.

Coupled QDs, in particular, have attracted much interest because the coupling and entanglement of quantized energy states between neighboring single QDs possess a potential application to quantum information devices [2, 3, 4, 5, 6]. However, the experimental studies of coupled QDs have been achieved mostly by using articulately engineered and prepared samples. For example, 'vertically' coupled QDs were fabricated by vertical alignment of a pair of QD layers [7, 8, 9, 10] and the measured energy splitting varied from several to several tens of meV depending on the barrier thickness between the upper and lower QDs in the bilayer QD structure [3, 11, 12]. The energy splitting has been also observed in 'laterally' coupled QD molecules, which were specially fabricated by cleaved edge overgrowth [2] or by combining molecular-beam epitaxy and atomically precise in-situ etching [13, 14, 15].

Self-assembled quantum dots, grown by molecular beam epitaxy, are usually highly dense with a density larger than 10^{10} cm^{-2}. Such a high-density sample of QDs has been widely studied as a natural candidate for applications to nano-optical devices. Although the spectroscopic and microscopic characteristics of self-assembled single QDs have been studied extensively, coupling between single QDs in such a *high-density* sample has not been investigated, obviously because it is difficult to discriminate the spectral as well as the spatial properties of their split energy states. Therefore, it will be an interesting challenge and significant progress to study coupling between two adjacent self-assembled QDs because of its inherent practical potentials for nano and quantum applications.

In this Letter, we report on the simultaneous spectroscopy and microscopy study of laterally coupled QDs in a self-assembled high-density InAs QD sample by using a near-field scanning optical microscope (NSOM), which has become a powerful tool to perform laser spectroscopy of single QDs [16, 17, 18]. The near-field fiber probe can measure the high-resolution optical properties of individual QDs in a high-density ensemble by detecting the

spectrally resolved photoluminescence (PL). Moreover, spatially resolved mapping of the PL-intensity images can clearly demonstrate that the bonding (symmetric) and antibonding (antisymmetric) energy states are associated with the lateral coupling of closely neighbored single QDs.

The self-assembled InAs QDs were grown on a GaAs substrate, having an average lateral dimension of 20 nm, a height of 2 nm, and a density of larger than 10^{10} cm^{-2}, with deposition of about two monolayers [19]. The QDs were capped by a 50 nm GaAs layer to reduce the contribution from carrier diffusion in the barrier layer. For the light source, we used the Ti:sapphire laser operating near 1.65 eV, which nonresonantly generates most of charge carriers in the GaAs cap layer. This excitation laser was coupled to a commercially available single-mode optical fiber and guided to a chemically etched sharp fiber tip, on which a 100-nm gold-coated aperture was fabricated [20]. Such a nanoscale light source generated by the apertured fiber probe could excite only a few tens of QDs by the shear-force distance control within several nm from the capping layer. The resulting PL was collected by the same fiber so that any loss of spatial resolution due to diffusion could be minimized [21]. The PL signal was then dispersed by a 30-cm long single monochromator with a spectral resolution of 0.3 meV and detected by a liquid-nitrogen-cooled charge coupled device (CCD) for high signal-to-noise ratio. Both the sample and the apertured fiber probe were enclosed in a He-flow-type cryostat and kept at about 10K.

Figures 1(a) and (b) present the typical time-integrated, high-resolution PL spectra of InAs QDs collected during 1 s with an 100-nm apertured probe at two different positions of the same sample. As can be observed, there are numerous sharp PL peaks associated with single QDs at a given position on the high-density sample. The four arrow markers in Fig. 1(a) indicate the selected PL energies at which the PL-intensity NSOM images are also presented; the corresponding NSOM images are shown in Fig. 1(c) to (f) for the PL peaks at (c) 1.2152 eV, (d) 1.2283 eV, (e) 1.2425 eV, and (f) 1.2601 eV.

The NSOM-image data-acquisition process is as follows: (1) The apertured probe is located on a given sample position and the PL spectrum is taken in the entire spectral range by the CCD camera during 1 s. (2) This data taking is repeated sequentially at all the 20×20 pixels of the 500 nm $\times$ 500 nm scanning area. (3) Each PL-intensity image at a given PL energy is then processed from the 400 data files, providing the corresponding energy spectra and spatial images of single QDs [18, 22, 23]. We employed the illumination-

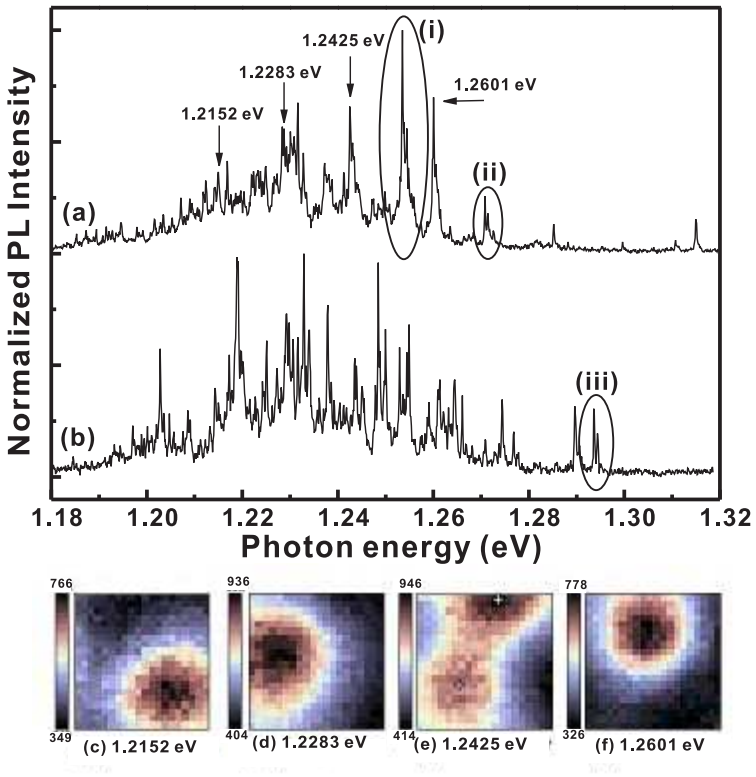

FIG. 1: Time-integrated PL spectra of high-density InAs single QDs obtained at two different detection positions of (a) and (b) on the same sample. PL-intensity NSOM images are shown for the four selected PL energies in (a), as marked by arrows; (c) 1.2152 eV, (d) 1.2283 eV, (e) 1.2425 eV, and (f) 1.2601 eV. The scan area is 500 nm $\times$ 500 nm.

collection mode of NSOM to obtain the high-resolution spatial PL-intensity images, from which one can clearly identify the isolated single QDs, as shown in Figs. 1(c), (d) and (f). On the other hand, as in Fig. 1(e), one can sometimes observe the spatial image of PL-intensity exhibiting two adjacent but independent single QDs having the same energy within the 0.3 meV resolution limit of the monochromator. The two cross symbols in Fig. 1(e) stand for the centers of the PL images of each QD and the distance between the two crosses is about 450 nm. This indicates that one can simultaneously observe the PL-intensity images of two separate single QDs with the same PL energies in a high-density sample. As is well known, the wave functions of two individual QDs can be overlapped as the lateral distance between the QDs is decreased [2, 24].

In order to study such possible electronic coupling between two neighboring QDs, we have

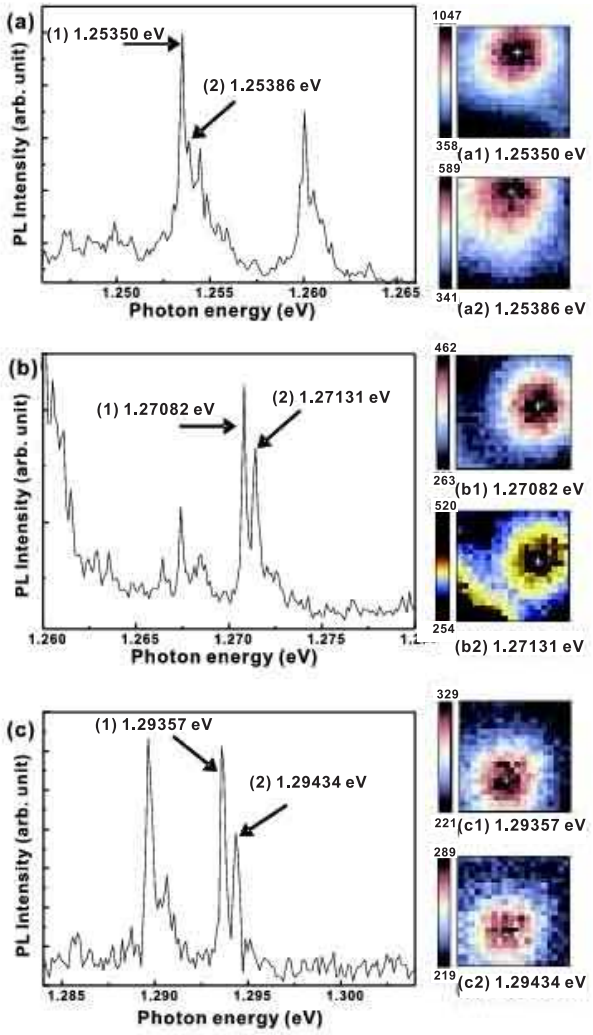

FIG. 2: Magnified view of the PL spectra shown in (a), (b) and (c), corresponding to those indicated by the three ellipsoids of (i), (ii) and (iii) in Figs. 1(a) and (b), respectively. The PL-intensity spatial images are also presented at the selected PL energies. The scan range is 500 nm × 500 nm.

further investigated the PL spectra which are slightly split, such as those indicated by the three ellipsoids in Figs. 1(a) and (b). The three selected PL spectra of (i), (ii) and (iii) in Figs. 1(a) and (b) are presented in detail in Figs. 2(a), (b) and (c), respectively. Each figure shows two slightly separated peaks, as arrow-marked by (1) and (2), whose corresponding spatial images are also presented on the right-hand sides as (a1), (a2), (b1), (b2), (c1) and (c2) in Fig. 2. In case of Figs. 2(a1) and (a2), although the PL energy difference is only 0.3 meV and thus is almost indistinguishable spectrally, the spatial PL-intensity images are rather distinguishable; the separation between the two crosses is about 75 nm (or three

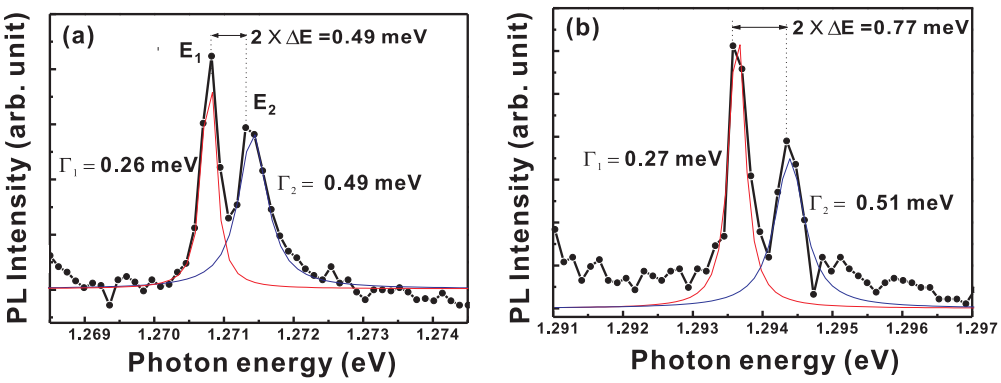

FIG. 3: Lorentzian fitting results for each PL peaks show the bonding (left-side curves) and antibonding (right-side curves) states for the two doublets in Figs. 2 (b) and (c). The differences between E_1 and E_2 are (a) 0.49 meV and (b) 0.77 meV, respectively. The linewidth of the doublet in (a) and (b) are (Γ_1 = 0.26 meV, Γ_2 = 0.49 meV) and (Γ_1 = 0.27 meV, Γ_2 = 0.51 meV), respectively.

pixels) with each image profile slightly different, depending on the specific wave-function of each single QDs having different size, shape, and strain [17, 18, 22, 23]. On the other hand, the centers of the PL-intensity images of Figs. 2(b1) and (b2) are located at the same position within one pixel of 25 nm, which limits the spatial resolution of our measurement. Moreover the two image profiles are very similar each other with a slightly split energy of 0.49 meV difference. The same conclusions also hold for the pair of Figs. 2(c1) and (c2), with a slightly increased PL-energy difference of 0.77 meV.

Figures 3(a) and (b) present the detailed Lorentzian line fittings for the doublet PL peaks of Figs. 2(b) and (c), respectively. The corresponding PL-energy splittings are 0.49 meV and 0.77 meV. The associated linewidths are obtained as; Γ_1 = 0.26 meV and Γ_2 = 0.49 meV for Fig. 3(a), whereas Γ_1 = 0.27 meV and Γ_2 = 0.51 meV for Fig. 3(b). From these results, one can observe that the linewidth of the higher energy PL state (Γ_2) is larger than that of the lower energy state (Γ_1), which is in qualitative agreement with the earlier observation in Ref. [2] where the broader linewidths were attributed to acoustic phonon scattering from the upper into the lower state of a simple two-level system. Note that the values of Γ_1 in Fig. 3 are slightly smaller than the spectral resolution limit (0.3 meV) of our measurement system, which indicates that the actual values of Γ_1 may be much smaller than 0.3 meV, as also observed in Ref. [2].

Johal *et al.* [24] reported that the edge-to-edge distance between a single dot and its nearest neighbor in the self-assembled, high-density QD structure is correlated with the dot size. In other words, the edge-to-edge distance between two adjacent QDs is decreased with the decrease of the QD diameter, which indicates that the smaller sized QDs are more strongly coupled laterally [24]. It is also well known that the higher PL energy is directly associated with the higher quantization energy of the smaller sized QD. Consequently, from these two facts, we may deduce that the coupled QDs are more easily observed at the PL energies higher than the average PL energy. For our sample, the average lateral size of single QDs is about 20 nm with the average PL energy of 1.23 eV, as shown in Fig. 1. Therefore, for the two coupled QDs having the PL energies of about 1.27 eV and 1.29 eV in Fig. 2 or Fig. 3, the size of those coupled QDs can be assumed to be smaller than 20 nm [18, 25, 26, 27]. Moreover, it can be justified that the doublet PL peaks in Figs. 2 (b) and (c) are not due to the internal energy states of a single QD, but result from the coupled states between a pair of interacting adjacent small-sized QDs, because the typical energy difference between the quantized energy states of a single InAs QD is several tens of meV [25, 26, 27], much larger than the energy splitting of about 1 meV in Fig. 2. It should be emphasized again that the results in Fig. 2(a) look like coupled QDs, but the PL-intensity images clarify that they are due to two uncoupled QDs having the similar energies, not from two coupled QDs located closely nearby.

Let us now make a qualitative description of the energy splitting in the laterally coupled QDs by a simple numerical analysis. In previous works, the doublet PL features such as those in Figs. 2 and 3 were explained as due to the excitonic emission of the bonding (symmetric) and antibonding (antisymmetric) states that result from the coupled ground states of independent single QDs [2, 24]; the energies of the bonding (E_1) and antibonding (E_2) states were expressed as $E_{1,2} = E_0 \mp \Delta E$ by the first perturbation theory. Here E_0 is the unperturbed energy of the individual QD and ΔE is the matrix element such that the coupling-induced energy splitting is $2 \times \Delta E$ [2]. Since the energy splitting ($2 \times \Delta E$) of the doublet states depends on the separation between two QDs as well as their size [2, 3], one may consider that the larger QDs with the lower PL energies are coupled in Fig. 3(a), whereas the smaller QDs with the higher PL energies are coupled in Fig. 3(b), as discussed before. Moreover, the exact distance between two coupled QDs cannot be directly measured because their separation is beyond the available spatial resolution limit of 25 nm. Nonethe-

less, for qualitative justification, we have performed a simple model calculation to estimate the distances between two coupled QDs.

In our analysis, each QD is modeled as a two-dimensional circular potential-well of diameter D,

$$V(r) = \begin{cases} -V_0 & \text{for } r < D/2, \\ 0 & \text{for } r > D/2. \end{cases} \tag{1}$$

For a single QD located at the origin, the normalized wave function of its electronic ground state is given by,

$$\psi_0(r) = \begin{cases} \mathcal{N} K_0(\kappa D/2) J_0(kr) & \text{for } r < D/2, \\ \mathcal{N} J_0(kD/2) K_0(\kappa r) & \text{for } r > D/2, \end{cases} \tag{2}$$

where $k^2 \equiv 2m_{\rm eff}(E_0 + V_0)/\hbar^2$, $\kappa^2 \equiv 2m_{\rm eff}|E_0|/\hbar^2$ ($m_{\rm eff}$ is the effective mass of electron), J_0 (K_0) is the zeroth-order (modified) Bessel function of the first (second) kind, and $\mathcal{N}$ is a normalization constant. Here the ground-state energy E_0 is determined by the lowest energy such that $kJ_1(kD/2)/J_0(kD/2) = \kappa K_1(\kappa D/2)/K_0(\kappa D/2)$. The bonding and antibonding states are then obtained by direct diagonalization of the Hamiltonian which describes two single QDs separated by the edge-to-edge distance of d. The diagonalization is performed in the Hilbert space spanned by the ground states of each QD. For our simulation, we used $V_0 = 0.6$ eV and $m_{\rm eff}/m_0 = 0.023$ (m_0 is the bare electron mass) [3, 7]. The diameter D of similar single QDs associated with each PL peaks in Fig. 3 can be also estimated from their PL energies; the PL energies of 1.271 eV and 1.294 eV correspond to the diameters D of 15.1 and 13.4 nm, respectively, because the average PL energy of 1.23 eV is attributed to the average diameter of $D = 20$ nm.

Figure 4 shows the computed energy splittings $2 \times \Delta E$ as a function of the edge-to-edge distance d for single QDs of various diameters D. The numerical curves then enable one to estimate the effective barrier width d (as shown in the inset of Fig. 4) from the experimental values of the energy splitting. We find that the coupled QDs in Figs. 3(a) and (b) correspond, respectively, to $d = 6.55$ and 6.47 nm, both smaller than the QD sizes, as expected. Therefore, by combining Figs. 2, 3 and 4, one may be able to investigate the doublet PL spectra of the bonding and antibonding states, as well as to estimate the separation of two coupled InAs QDs embedded in a 50 nm GaAs capping-layer.

In conclusion, we have employed the PL NSOM method to obtain spatially and spectrally resolved PL-intensity images due to *laterally coupled* single QDs in a self-assembled, high-

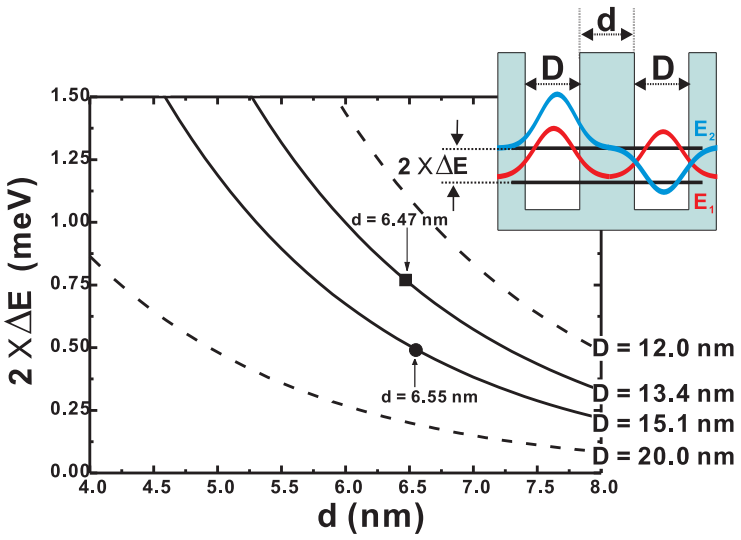

FIG. 4: Calculated results of correlation between the energy splitting (2×ΔE) and the edge-to-edge distance (d) of coupled QDs for various QD diameters (D = 12.0 nm, 13.4 nm, 15.1 nm and 20 nm). The inset is the schematic diagram of the split bonding (symmetric) and antibonding (antisymmetric) ground-states of the coupled QDs.

density QD sample. In particular, the high-resolution PL spectra and the PL-intensity images exhibit the bonding and antibonding states associated with two coupled, closely adjacent QDs. By a simple model calculation, we have also estimated the separations between coupled QDs. This work may open the possibility to investigate the coupling interactions between closely neighboring QDs in a high-density QD sample for quantum optics or quantum information applications with the simultaneous high spectroscopic as well as microscopic resolution.

Acknowledgments

This work was supported by the Korean Ministry of Science and Technology.

[1] H. Haken, and H. C. Wolf, *The Physics of Atoms and Quanta; Introduction to Experiments and Theory* (Springer-Verlag, 2000).

[2] G. Schedelbeck *et al.*, Science **278**, 1792 (1997).

[3] M. Bayer *et al.*, Science **291**, 451 (2001).

[4] S. Lloyd, Sci. Am. **273**, 140 (1995).

[5] A. Barenco *et al.*, Phys. Rev. Lett. **74**, 4083 (1995).

[6] P. Borri *et al.*, Phys. Rev. Lett. **87**, 157401 (2001).

[7] M. Korkusinski and P. Hawrylak, Phys. Rev. B **63**, 195311 (2001).

[8] G. Bester *et al.*, Phys. Rev. B **71**, 075325 (2005).

[9] B. D. Gerardot *et al.*, Phys. Rev. Lett. **95**, 137403 (2005).

[10] K. Goshima *et al.*, Appl. Phys. Lett. **87**, 253110 (2005).

[11] T. Fujisawa *et al.*, Science **282**, 932 (1998).

[12] L. R. C. Fonseca *et al.*, Phys. Rev. B **58**, 9955 (1998).

[13] R. Songmuang *et al.*, Appl. Phys. Lett. **82**, 2892 (2003).

[14] B. Krause *et al.*, Phys. Rev. B **72**, 085339 (2005).

[15] G. J. Beirne *et al.*, Phys. Rev. Lett. **96**, 137401 (2006).

[16] A. Chavez-Pirson *et al.*, Appl. Phys. Lett. **72**, 3494 (1998).

[17] K. Matsuda *et al.*, Phys. Rev. Lett. **91**, 177401 (2003).

[18] Y.-J. Yu *et al.*, Appl. Phys. Lett. **87**, 143108 (2005); Y.-J. Yu *et al.*, *ibid.* **83**, 3024 (2003).

[19] Y. Toda *et al.*, Appl. Phys. Lett. **73**, 517 (1998).

[20] M. Ohtsu, *Near-Field Nano/Atom Optics and Technology*, (Springer-Verlag, 1998).

[21] T. Saiki, and K. Matsuda, Appl. Phys. Lett. **74**, 2773 (1999).

[22] Y.-J. Yu *et al.*, Jpn. J. Appl. Phys. **45**,656 (2006).

[23] S.-K. Eah *et al.*, Appl. Phys. Lett. **80**, 2779 (2002).

[24] T. K. Johal *et al.*, Phys. Rev. B **66**, 155313 (2002).

[25] L. Brusaferri *et al.*, Appl. Phys. Lett. **69**, 3354 (1996).

[26] Y. C. Zhang *et al.*, J. Appl. Phys. **90**, 1973 (2001).

[27] H. Kissel *et al.*, Phys. Rev. B **62**, 7213 (2000).